nature COMMUNICATIONS

ARTICLE

Received 28 May 2013 | Accepted 25 Nov 2013 | Published 7 Jan 2014

DOI: 10.1038/ncomms4023 OPEN

Orthogonally modulated molecular transport junctions for resettable electronic logic gates

Fanben Meng[1], Yves-Marie Hervault[2], Qi Shao[1], Benhui Hu[1], Lucie Norel[2], Stéphane Rigaut[2] & Xiaodong Chen[1]

Individual molecules have been demonstrated to exhibit promising applications as functional components in the fabrication of computing nanocircuits. Based on their advantage in chemical tailorability, many molecular devices with advanced electronic functions have been developed, which can be further modulated by the introduction of external stimuli. Here, orthogonally modulated molecular transport junctions are achieved via chemically fabricated nanogaps functionalized with dithienylethene units bearing organometallic ruthenium fragments. The addressable and stepwise control of molecular isomerization can be repeatedly and reversibly completed with a judicious use of the orthogonal optical and electrochemical stimuli to reach the controllable switching of conductivity between two distinct states. These photo-/electro-cooperative nanodevices can be applied as resettable electronic logic gates for Boolean computing, such as a two-input OR and a three-input AND-OR. The proof-of-concept of such logic gates demonstrates the possibility to develop multifunctional molecular devices by rational chemical design.

[1] School of Materials Science and Engineering, Nanyang Technological University, 50 Nanyang Avenue, Singapore 639798, Singapore. [2] Institut des Sciences Chimiques de Rennes, UMR 6226 CNRS—Université de Rennes 1, 263 Avenue du Général Leclerc, F-35042 Rennes cedex, France. Correspondence and requests for materials should be addressed to S.R. (email: stephane.rigaut@univ-rennes1.fr) or to X.C. (email: chenxd@ntu.edu.sg).

Since the first molecular rectifier proposed in 1974 (ref. 1), functional devices developed with individual molecules as functional components have exhibited promising applications in the fabrication of computing nanocircuits. Their advantages lie in synthetic tailorability, chemically controllable assembly, scalable size, and so forth[2]. As an essential structure in molecular electronics, molecular transport junctions (MTJs) have been used to investigate electronic conduction through functional molecules[3–6]. As a result, many electro-active properties, such as rectification[7,8], negative differential resistance[9,10] and Coulomb blockade[11], have been uncovered, indicative of their promising applications in functional electronic devices. Additionally, external stimuli, such as light[12–16], mechanical force[17,18], magnetic field[19,20], electrical field[21–23] and electrochemical potential[24–28], were introduced to modulate the molecular conductivity and thus to tune the properties of functional molecular devices, thereby significantly driving their development. As attested by the giant magnetoresistance effect[29,30] and photoelectric cooperation[31,32], a better synergy between such external stimuli and corresponding fabrication of multi-addressable MTJs may further efficiently advance the field of molecular electronics. Therefore, herein, we will take the advantages of synergetic modulation by multiple external controls, to explore multi-modulable molecular devices, which have not been addressed so far.

In this respect, chemical tailoring of functional molecules with multi-addressable properties will serve as an effective approach to fabricate such molecular devices. In order to address this issue, we designed and synthesized a new family of organometallic compounds, combining an ideal dithienylethene (DTE) photochromic unit[33,34] and a unique electro-active carbon-rich ruthenium complex[35–39], targeting multifunctional switching properties addressable with photon and/or electrons[40–43]. In a recent work[44], we showed that the bimetallic compound **1** bearing two ruthenium fragments $[AcS–C_6H_4–C{\equiv}C(dppe)_2Ru]^+$ (dppe = 1,2-bis(diphenylphosphino)ethane) on either ends of a DTE unit exhibits the reversible photo-controllable switching of conductivity when placed within a pair of gold nanoelectrodes fabricated by on-wire lithography (OWL)[45–47]. In such a molecular wire, the DTE unit undergoes photo-isomerization

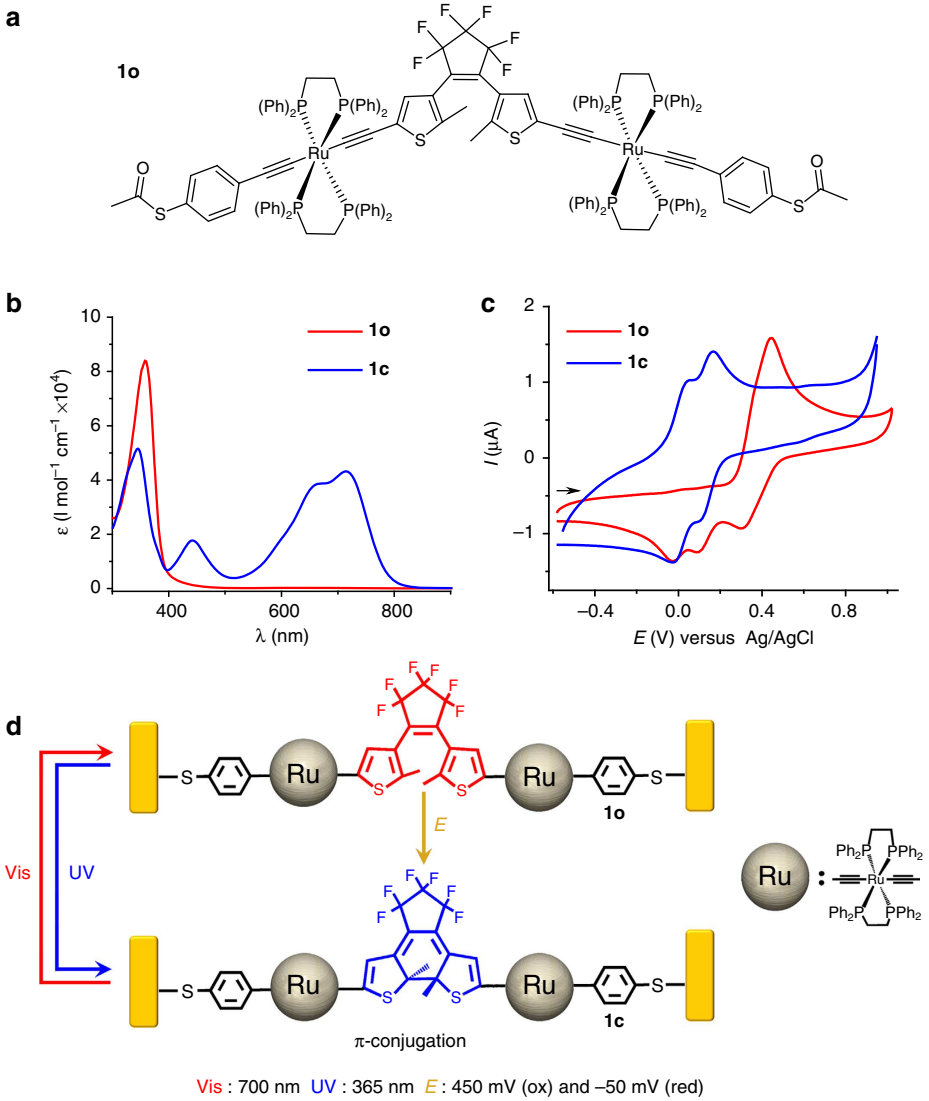

Figure 1 | Orthogonally modulated isomerization of 1. (**a**) Chemical structure of **1o**. (**b**) Absorption spectra and spectral changes upon 350 nm irradiation of **1o** (50 μM in toluene). The process is fully reversible upon irradiation of **1c** at 750 nm. (**c**) CV of **1o** in CH_2Cl_2 (0.2 M Bu_4NPF_6) before (red line) and after irradiation at 350 nm leading to **1c** (blue line), scan rate 0.1 V s^{-1}. (**d**) Scheme of molecular isomerization of **1** under external controls. E, electrolysis; UV, UV irradiation; Vis, visible light irradiation.

between a π-conjugated closed state (**c**) and a non-conjugated open state (**o**), and thus dominates the conductive state of the nanodevice, while the ruthenium moieties properly modulate electronic coupling between this DTE moiety and Au electrodes to avoid one-way switching[48]. In addition to this photochromic property, we previously showed that such a ruthenium/DTE association can also perform electrochemical cyclization of the DTE unit in solution at low potential[40], in contrast to organic systems[49,50]. Therefore, since it has been successfully demonstrated that molecular conductance can be respectively tuned by light irradiation[12–16,44] or electrochemical potential[24–28], we were strongly motivated in the association of these two stimuli in a single electronic device to achieve orthogonally modulated MTJs.

In this contribution, we report for the first time the photo- and electro-commutation of MTJs based on OWL-generated nanogaps modified with two Ru/DTE complexes. First, the reversible and repeatable conductivity switching can be achieved upon orthogonal optical and/or electrochemical triggering of the molecular isomerization of **1o**, thanks to the remarkably low potential for electrochemical cyclization allowing the maintenance of stable thiol linking bonds at electrode interface. Then, a new longer trimetallic complex with two DTE units is designed towards a multi-addressable system and to further improve device complexity. It results in the fact that the corresponding device can achieve an original stepwise control of conductance requiring both stimuli. Finally, with a judicious choice of photo-/electro-inputs, OR and AND-OR Boolean computing are achieved within the orthogonally modulated MTJs.

Results

Optically and electrochemically co-modulated MTJs. The binuclear compound **1** (Fig. 1a) can achieve photo-triggered isomerization both in solution and in solid-state nanodevices. As previously demonstrated[44], reversible photochromic processes are achieved upon irradiation with UV light for ring closure and visible light for ring opening in solution (Fig. 1b). A typical cyclic voltammogram (CV) of **1o** is also shown on Fig. 1c. It presents a partially reversible wave at $E_{pa} = 480$ mV versus Ag/AgCl composed of two slightly separated one-electron oxidations for the two electronically independent metal fragments leading to $\mathbf{1o}^{2+}$. During the reverse cathodic scan, two new waves appear at less positive potentials and are ascribed to the $\mathbf{1c}^{+}/\mathbf{1c}$ and $\mathbf{1c}^{2+}/\mathbf{1c}^{+}$ processes involving the closed isomer electrochemically generated due to radical coupling as observed with its parent complex (Supplementary Fig. 1)[40]. Logically, identical waves are obtained after photolysis ($\lambda = 350$ nm) of **1o**, that is, at $E°_{c1} = 16$ mV and $E°_{c2} = 144$ mV, along with the vanishing of the wave at ca. 480 mV. Therefore complex **1** is an ideal candidate to explore photo-/electro-switchable MTJs when incorporated into a pair of nanoelectrodes, as illustrated in Fig. 1d, which is also strongly supported by the theoretical calculations of molecular geometric reorganization and transmittance process through the molecule[44].

OWL-generated gap-based nanodevices have been demonstrated as a unique testbed for molecular electronics[51–54]. In order to apply optical and electrochemical stimuli to functional molecules, the nanogap devices are further incorporated with one fluidic cell to achieve an electrochemical environment for device modulation, as shown in Fig. 2a. Electrochemical processes were carried out using a gold nanorod on one side of nanogap as the working electrode with a diameter of ~300 nm, a Pt wire as counter electrode and a homemade AgCl coated Ag wire as reference electrode (Fig. 2a). In a typical experiment, complex **1c** was covalently bonded onto the two sides of OWL-generated

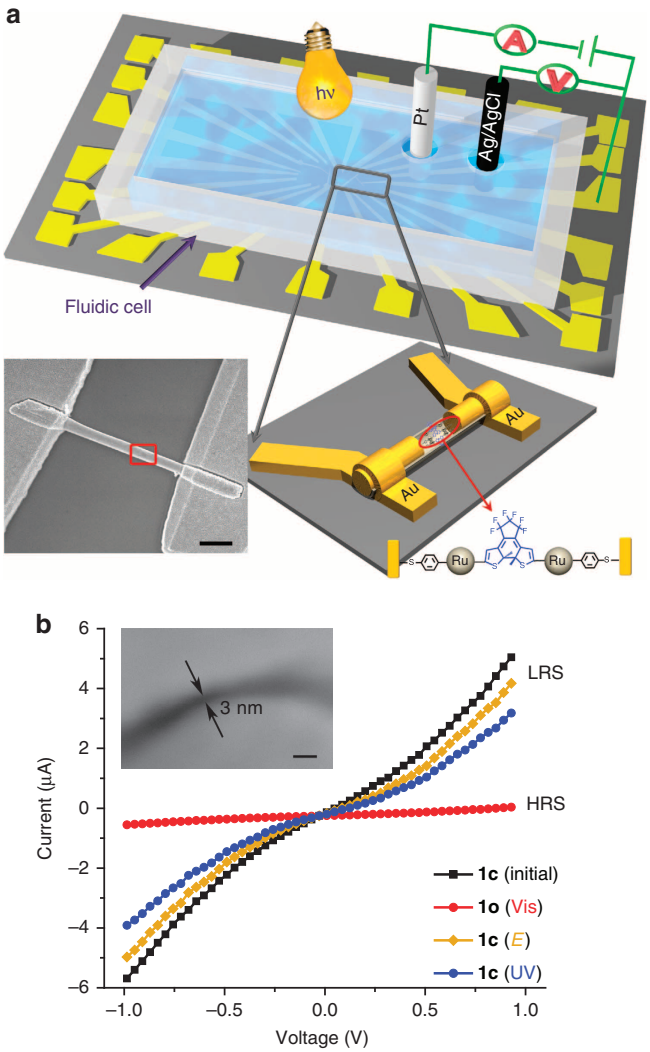

Figure 2 | 1c-functionalized nanogap devices. (**a**) Diagram of the functionalized nanogap devices. Inset: SEM image of a device fabricated by OWL-generated nanowire (scale bar: 1 μm). (**b**) *I*–*V* characteristics of ~3 nm gap devices loaded with **1c**, and obtained in the dark under vacuum. Black curve: initial **1c** device. Red curve: after 700 nm irradiation of **1c** device for 2 h to **1o** device. Yellow curve: after subsequent electrolysis of **1o** at 450 mV versus Ag/AgCl for 10 min followed by −50 mV for 10 min in CH_2Cl_2 to return to **1c** device. Blue curve: after 365 nm irradiation of **1o** device for 30 min to obtain the **1c** device. Inset: SEM image of a ~3 nm gap (scale bar: 10 nm).

~3 nm gaps (Fig. 2b, inset) after deprotection of the thiol, to ensure the accurate electronic coupling between the molecule and electrodes[51,54]. As expected, a photo-triggered conductive switching from low resistance state (LRS, Fig. 2b black curve) to high resistance state is observed (HRS, Fig. 2b, red curve) upon 700 nm irradiation, leading to the photochemical isomerization of π-conjugated **1c** to non-conjugated **1o**. The reverse process switches back the device to LRS via the photochemical closure upon UV light irradiation (365 nm) (Fig. 2b, blue curve).

Subsequently, electrochemical cyclization was also attempted with a device loaded with **1o** molecules by applying a positive potential of 450 mV versus Ag/AgCl followed by a slightly negative potential (−50 mV), in CH_2Cl_2 solution. For enabling comparison with photochemical processes, electrical measurements were then carried out in vacuum after removing CH_2Cl_2, in order to eliminate the influence of the solvent on the device

conductivity and to only obtain information on molecular resistance (Supplementary Fig. 2). Thus, as attested by the resultant switching to the high conduction state (Fig. 2b, yellow curve), the electrochemical ring closure was successfully realized. By analogy with what occurs in solution, after applying a potential of 450 mV, it is anticipated that **1o** within the nanogap is oxidized to $\mathbf{1o}^{2+}$. Then, $\mathbf{1o}^{2+}$ undergoes radical coupling to form the more stable isomer $\mathbf{1c}^{2+}$, which is further reduced to **1c** by the slightly negative potential (-50 mV) applied subsequently. Importantly, due to the unique electronic structure of the ruthenium fragment, this electrochemical cyclization in the nanogap can be achieved at a low potential, avoiding the breakage of the Au–S bond, which is not possible in the case of pure organic DTE (>1 V potential is needed to perform ring closure)[49,50]. Moreover, this electrochemically obtained LRS state could be switched back to the initial HRS state (open state) upon visible light irradiation as described above.

MTJ-based resettable electronic logic gates. Based on its unique orthogonally modulable property, the **1**-functionalized MTJs can be viewed as an electronic logic gate (Fig. 3a). The LRS **1c**-based device is first set to HRS (**1o**) by irradiation of 700 nm light. Then, the UV light irradiation and electrochemical stimulus are employed as inputs. The presence and absence of each input is respectively defined as '1' and '0'. The outputs ('1' for LRS and '0' for HRS) can be recorded by the conductance change from the previous HRS devices to the modulated devices. As shown in Fig. 3b, except in the case of absence of both inputs (0, 0), which leaves the device in HRS (output = 0), the presence of either (0,1 or 1,0) or both inputs (1,1) could all trigger the molecular arrangement from the open state to the π-conjugated closed state, resulting in the enhancement of device conductivity to LRS (output = 1). Hence, the Boolean computing of OR (Fig. 3c) has been achieved with the **1c**-functionlized nanodevices. In addition, a distinct advantage of such functional MTJs as logic gates is the

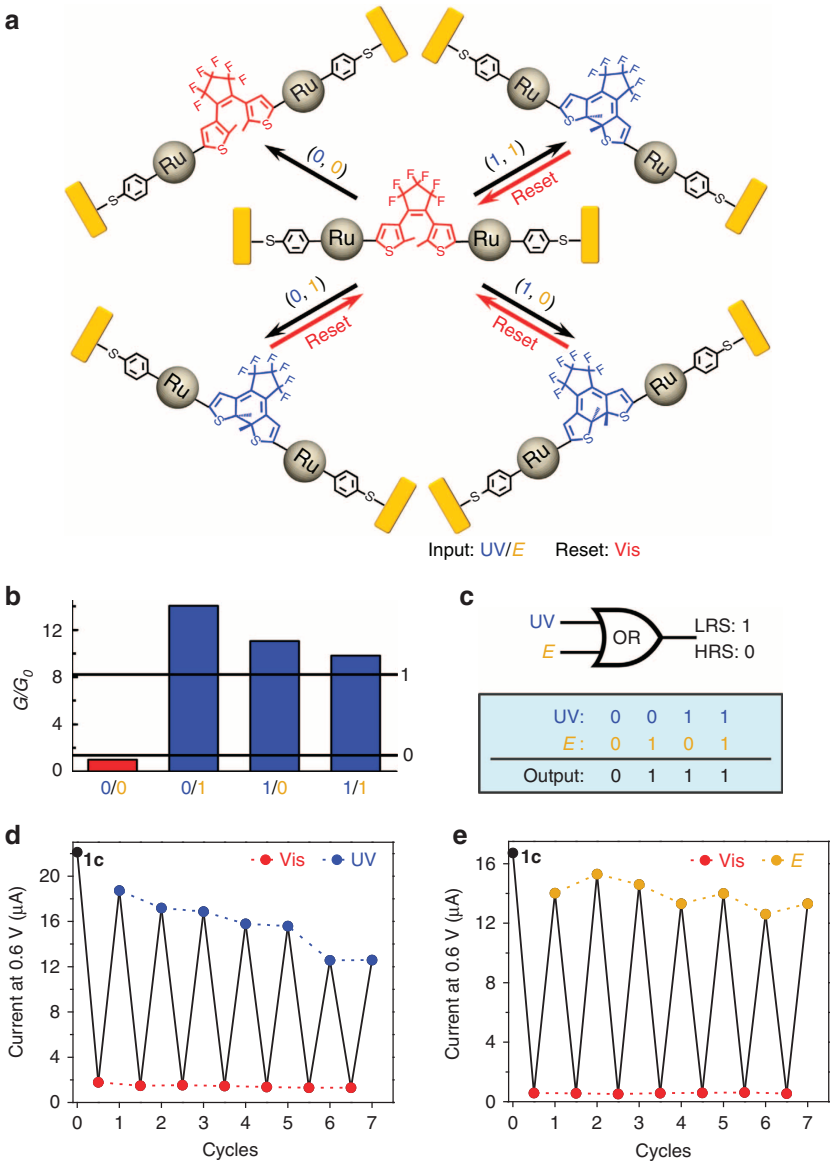

Figure 3 | Resettable OR logic gate using 1c-based MTJs. (**a**) Scheme of **1**-based logic gate: **1** isomerization within nanogap devices under different inputs (UV irradiation and electrolysis). Reset: visible light irradiation (700 nm, 2 h). (**b**) Conductance (G) changes with different input combinations. (**c**) The electronic symbol and a truth table of the OR logic gate. (**d**,**e**) Endurance performance: current response of a **1c**-based nanodevice under alternate modulation of visible light irradiation (700 nm for 2 h) and (**d**) UV irradiation (365 nm for 30 min) or (**e**) Electrochemical stimuli (oxidation at 450 mV and reduction at -50 mV for 10 min). The current values were recorded at 0.6 V bias in vacuum.

resettability. Upon irradiation under visible light (700 nm), this nanodevice can be reset from LRS (1) to HRS (0). Thus, to illustrate the feasibility of these resettable MTJs as operative electronic devices, the reversibility and repeatability under the two different external stimuli have been investigated. As shown in Fig. 3d,e, the two distinct states of the device conductivity can be clearly observed after different cycles. The reversible photo- and electro-triggered resistive switching can be repeatedly operated for several cycles and it maintains a bi-state system, indicating the potential application of such a device in resettable electronic logic gates. As previously reported by us[44] and others[12–16], a progressively reduced reversibility in the course of a cycling test using the photochemical stimuli was observed (Fig. 3d). As the conductance of the devices showed no obvious change but rather just regular fluctuations with several electrochemical modulations (Fig. 3e, yellow dots), it can be concluded that UV irradiation is responsible for decomposition of some molecules and of the subsequent conductance drop (Fig. 3d, blue dots), rather than desorption of molecules from the gold surface due to stochastic behaviour of thiols[55,56] or mechanical breaking of bonds upon isomerization as previously proposed. Consequently, the electrochemical control appears to be more reliable in maintaining a stable conductance. Another possible reason for the reduced reversibility, especially comparing with the initial device state, is that some molecules are connected in the nanogap with some constraints due to the roughness of the gap or interactions with other molecules. The first opening process can reduce these constraints and thus further re-closing is not favourable. Nevertheless, herein, an OR logic gate has been developed by the orthogonally modulated MTJs. In contrast to other logic gates based on chemical systems[57–60], such molecular nanodevices exhibit unique advantages of resettablity[61,62]. Additionally, direct electronic outputs will be more convenient for nanocircuit construction compared with other outputs such as optical signals that have arisen from a similar complex[43,63].

Multi-addressable MJTs for advanced Boolean computing. In order to explore more advanced functions toward multi-addressable light and electro-triggered multifunctional objects and to increase device complexity, the new trinuclear compound **2oo** was designed, as is depicted in Fig. 4a. It was readily achieved using the similar synthetic pathway to that used for the previously reported analogue complex without the protected linking functions[41]. **2oo** was fully characterized and shows characteristics similar to those of the latter. In particular, isomerization studies unambiguously show that the photochromic conversion of **2oo** to the very stable **2cc** complex upon irradiation is complete and fully reversible (Fig. 4b). More specifically, the colourless complex **2oo** displays an absorption at $\lambda_{max} = 357$ nm, and upon irradiation with UV light (350 nm), this band vanishes while a broad absorption assigned to the deep green closed isomer **2cc** appears at $\lambda_{max} = 733$ nm. This solution can be further bleached back to the colourless solution of **2oo** under visible light (750 nm) via ring opening. During light irradiation, the intermediate **2co** is just transitorily formed and cannot be isolated, as already demonstrated with the related complex[41]. A typical CV of **2oo** is shown in Fig. 4c that presents a similar wave to that of **1o** at $E_{pa} = 500$ mV versus Ag/AgCl composed of three slightly separated one-electron oxidation for the three electronically independent metal fragments leading to $\mathbf{2oo}^{3+}$. During the reverse cathodic scan, two new waves appear at less positive potentials and are ascribed to the $\mathbf{2oc}^{+}/\mathbf{2oc}$ and $\mathbf{2oc}^{2+}/\mathbf{2oc}^{+}$ processes for the open–closed isomer electrochemically generated (Supplementary Fig. 3), since only one radical coupling could be obtained with oxidation of three Ru centres[41]. The CV of **2cc** is obtained after photolysis ($\lambda = 350$ nm) of **2oo**, and presents four systems at $E^{\circ}_{c1} = 94$ mV, $E^{\circ}_{c2} = 210$ mV, $E^{\circ}_{c3} = 330$ mV and $E^{\circ}_{c4} = 500$ mV. Thus, as illustrated in Fig. 5a, **2oo** displays the same unique properties as those of its parent compound without the linking functions, and is thereby a multi-addressable light and electro-triggered multifunctional object for integration in nanogaps. Of particular interest is the stepwise ring closure:

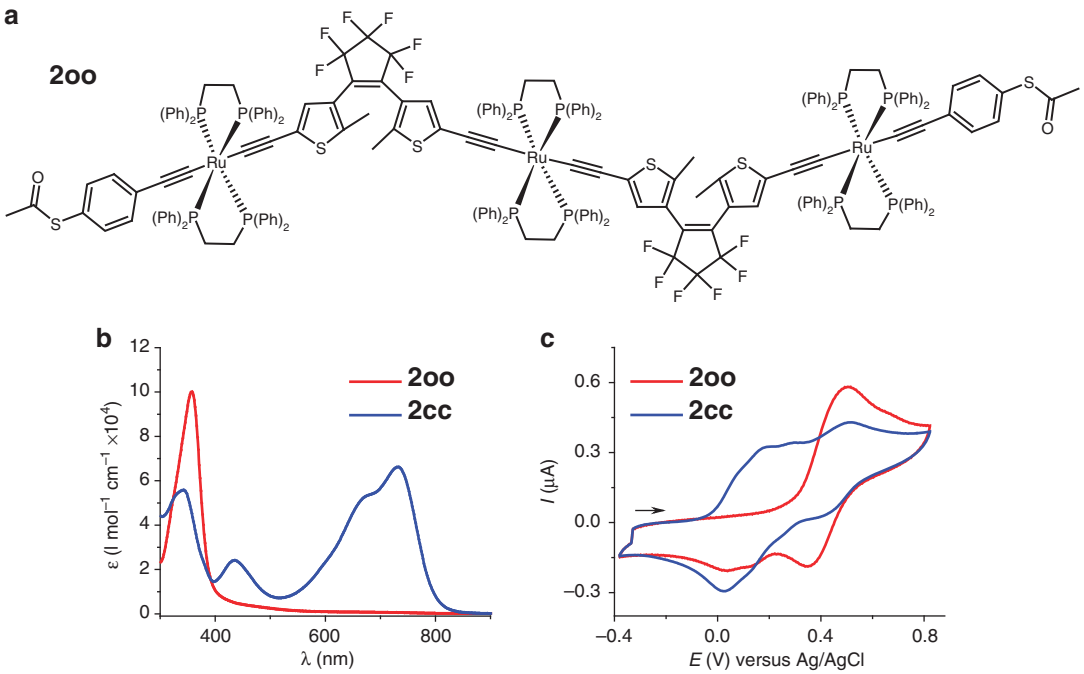

Figure 4 | Orthogonally modulated isomerization of 2. (**a**) Chemical structure of **2oo**. (**b**) Absorption spectra and spectral changes upon 350 nm irradiation of **2oo** (50 μM in toluene). The process is fully reversible upon irradiation of **2cc** at 750 nm. (**c**) CV of **2oo** in CH_2Cl_2 (0.2 M Bu_4NPF_6) before (red line) and after irradiation at 350 nm leading to **2cc** (blue line), scan rate 0.1 V s^{-1}.

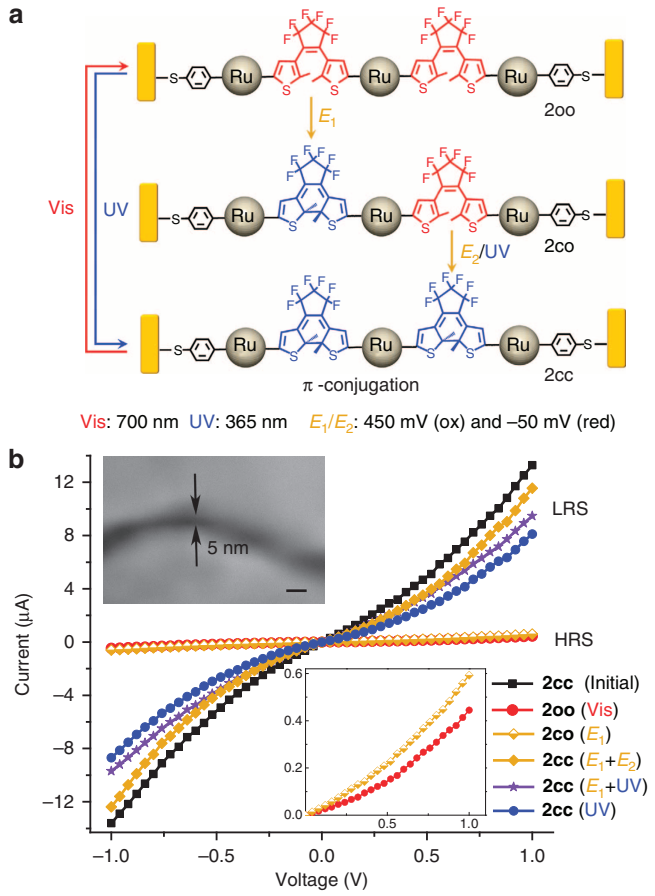

Figure 5 | 2cc-functionlized nanogap devices. (**a**) Scheme of molecular isomerization of **2** under external controls. E_1 and E_2, two cycles of electrolysis; UV, UV irradiation; Vis, visible light irradiation. (**b**) *I–V* characteristics of a ~5-nm gap device loaded with **2cc** under vacuum. Black curve: initial **2cc** device. Red curve: after 700 nm irradiation of **2cc** for 2 h to **2oo** device. Half yellow curve: the resulting **2co** device after one step of electrolysis of the **2oo** device at 450 mV versus Ag/AgCl for 10 min followed by −50 mV for 10 min in CH_2Cl_2. Yellow curve: after two cycles of such electrolysis of **2oo** to achieve the **2cc** device. Purple curve: one electrolysis cycle of **2oo** followed by 365 nm irradiation for 30 min to achieve the **2cc** device. Blue curve: 365 nm irradiation of **2oo** for 30 min to **2cc** device. Inset: SEM image of ~5 nm gap (scale bar: 10 nm).

after electrochemical oxidation followed by reduction to the neutral state, a single ring closure leads to **2oc**, and further full closure to **2cc** can thus be accomplished electrochemically or with UV light[41].

Complex **2cc** was further assembled into OWL-generated ~5 nm gap devices (Fig. 5b, inset), under the same condition as those used for **1c** immobilization. The gap size here was tailored to be consistent with the length of **2cc** that was estimated to ca. 49 Å using molecular model based on the bimetallic parent complex[40,44]. As shown in Fig. 5b, a characteristic *I–V* response has been observed with the symmetric black curve, which represented the successful formation of **2cc**-based transport junctions. As observed with **1c**-based device, the conductivity of the **2cc**-based nanodevices decreased after irradiating with 700 nm visible light (Fig. 5b, red curve), corresponding to the molecular isomerization from the fully π-conjugated **2cc** (LRS) to the non-conjugated **2oo** (HRS). Then, molecule **2** can also undergo the fully reverse photo-isomerization upon UV irradiation, and directly interchange from **2oo** to **2cc** through the transitory **2oc**. The device is then tuned back from HRS to LRS (Fig. 5b, blue curve).

More interestingly, further application of the electrochemical stimuli defined as E_1 (sequentially applying 450 mV for oxidation of the organometallic ruthenium moieties, and −50 mV for reduction of the complex to the neutral state) to the **2oo**-based nanodevice, to perform DTE ring closure as for **1o**-based devices, led to no significant change in the conductance of the device. Only a slight increase could be observed as shown by the half yellow curve in Fig. 5b. This expected fact is attributed to a single DTE electrochemical cyclization of **2oo** to **2co**, since only one ring closure is obtained via one radical coupling in the triply oxidized molecule $\mathbf{2oo}^{3+}$ to provide $\mathbf{2co}^{3+}$ before reduction, as stated above[41]. Thus, in this case, the non-conjugated open DTE unit dominates the resistance of the whole molecule and the device is maintained in the HRS state. Starting from this **2co** state, the conductivity jumps to the LRS when the device is further exposed to 365 nm UV irradiation (Fig. 5b, purple curve), as expected, leading to the **2cc**-based nanodevice. Significantly, when the **2co**-device is further submitted to another electrochemical cycle (also sequentially applying 450 mV, and −50 mV), defined as E_2, under the same conditions as the first (Fig. 5b, yellow curve), the LRS is also reached. These results indicated that two DTE units are fully closed and that the π-conjugated **2cc** is also formed within the nanogap in both cases. Thus, in addition to the one-step UV irradiation, the full molecular isomerization of **2oo** to **2cc** in the nanogap can be also achieved by stepwise and orthogonal electrochemical and photo stimulations or via a two-step electrochemical process, most likely via two stepwise radical couplings of the two DTE units. It should be noted that owing to the unique gap structure of this nanodevice, the two opposite nanorods of the gap can both be employed as working electrodes for electrolysis, and therefore the later step can be achieved using the same or the opposite nanoelectrodes.

As discussed with **1c**, **2cc**-functionalized MTJs can also be designed for Boolean operation (Supplementary Fig. 4). Upon 700 nm light irradiation, the **2cc**-functionalized device is set to the **2oo**-based HRS. Electrochemical modulation and UV irradiation for ring closures can be employed as inputs. First, without introduction of 365 nm UV light irradiation (UV: 0), the presence and absence of each of the electrochemical input step (E_1 and E_2) were defined as '1' and '0'. Only the presence of both inputs (1, 1) could cause the two stepwise ring closure to form π-conjugated pattern of **2cc**, promoting the electron transport (output = 1); while in absence of both (0, 0) or either inputs (1,0 or 0,1), the device conductivity remain as HRS (output = 0) (Fig. 6a). These results suggest that an electronic AND gate has been achieved with only stepwise electrochemical modulations. It is worth noting that although the device remained in HRS with the inputs of (0, 0), (0, 1) or (1, 0), the molecular structure is not the same in all cases. By one-step electrochemical modulation, **2oo** likely completed a single ring closure to form **2co**. As discussed above, in this case, only slight conductance enhancement was observed and the device remained in HRS. On the other hand, when the UV irradiation as the third terminal input (UV: 1) was used, **2oo** could undergo the photo-isomerization to **2cc** by closure of two DTE units simultaneously, and therefore the device were directly tuned from HRS to LRS (Fig. 6a), irrespective of any electrochemical stimuli being applied. Hence, a more complicated three-terminal logic gate has been developed combining the sequential Boolean computing AND and OR. (Fig. 6b)

Then, this functionalized three-terminal logic gate is also resettable with the help of 700-nm irradiation. Therefore, as shown in the Fig. 6c,d, both photo- and electro-triggered conductive switching could be repeatedly operated. Note that the progressively reduced reversibility in Fig. 6c also suggests that

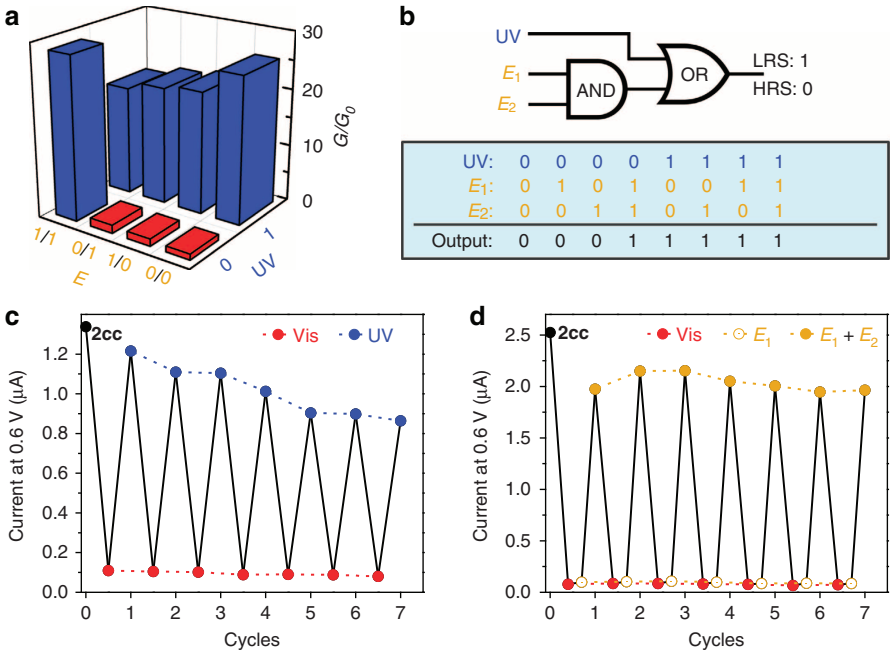

Figure 6 | Resettable AND-OR logic gate based on 2cc-based MTJs. (**a**) Conductance (*G*) changes with different input combinations. (**b**) The electronic symbol and a truth table of the AND-OR logic gate. (**c**,**d**) Endurance performance: current response of a **2cc**-based nanodevice under alternate modulation of visible light irradiation (700 nm for 2 h) and (**c**) UV irradiation (365 nm for 30 min) or (**d**) two successive electrochemical cycles (oxidation at 450 mV and reduction at −50 mV for 10 min). The current values were recorded at 0.6 V bias in vacuum.

UV irradiation may cause decomposition of some functional molecules with time. In contrast, the stepwise electrochemical modulations clearly exhibit reversibility in Fig. 6d. This fact highlights the pertinence of our electrochemically driven ruthenium/DTE nanodevices. Note that owing to the sensitivity of UV irradiation, the stability of such logic devices is not yet competitive to conventional semiconductor devices. However this first proof-of-concept of MTJ-based logic devices will push forward the development of such multifunctional molecular devices.

Discussion

It is worth noting that the yield of operative devices was ~21% (18/86 on a single chip of 1 cm × 1 cm, Supplementary Table 1) for **1c**-functionalized devices and 17% (13/77 on a single chip of 1 cm × 1 cm, Supplementary Table 2) for **2cc**-functionalized devices. For different operative devices, a disparity in conductivity can be observed (current range: $\sim 10^{-5}$ to $\sim 10^{-9}$ A, at 1 V bias). This disparity should be mainly ascribed to the different number of functional molecules that actually span the nanogaps from one to the other[44], which may be due to the ±0.2 nm gap size variation, and the uncontrollable roughness and morphology of the gold surface[51–53]. As estimated on the diameter of molecules[44], up to $\sim 3 \times 10^4$ molecules can be ideally assembled in the junction (see experimental methods for detail), which is according to the four orders of magnitude range of the measured currents. As similar conductivity disparity can be found in the other reported molecular junctions based on the OWL-generated nanogap[51–53], and considering the different size and resistance of single functional molecules, all these highly agreed with each other. In addition, the lowest observed current magnitude is at ~nA level that corresponds to the junction with only few molecules loaded, which is comparable to the results of single-molecule studies in previous reports on shorter DTE-containing molecules[13,34]. Besides the conductivity disparity, the current ratios between '1' and '0' states of different devices exhibit a slight fluctuation (Supplementary Tables 1 and 2). However, these ratios are all located in the range of 10–20 times, which are consistent with theoretical[44] or experimental[13,34] closed/open current ratios of single DTE derivatives, taking into account the high number of molecules loaded in the nanogaps. Such random fluctuation may be ascribed to slightly different orientations and conformations of functional molecules within each working device with variable roughness affecting the efficiency of the switching events. Note that the logic nanodevices presented here show a longer switching time compared with the traditional semiconductor systems, especially during photo-stimulation. This issue should be significantly improved through quantity control of assembled functional molecules within the junction since molecular number also determines the photostationary switching time upon light irradiation[64], and amelioration of the device design for the irradiation procedure. Therefore, there is a lot of room for improvements in the optimization of device fabrication and functional molecule assembly to fit the potential application of complex logic computing in future studies.

In summary, we have demonstrated the achievement of multi-modulated MTJs based on the association of original ruthenium/DTE complexes and OWL-fabricated nanogaps with suitable gap sizes. The devices represent the very first molecular nanodevices that perform bi-state switchable conductivity by judicious control of the orthogonal light irradiation and electrochemical stimuli. The successive structural rearrangement of the incorporated molecules, that is, the photo-triggered reversible isomerization and especially the low-potential electro-triggered metal-promoted electrochemical cyclization, are all based on rational molecular design that allows stable Au–S bond connection between the functional molecules and two nanoelectrodes. Remarkably, the unique electronic structure of the longer molecule combining two DTE units offered the achievement of stepwise modulation. Therefore, depending on the properties of orthogonal modulation, these multi-addressable MTJ-based nanodevices can be designed to achieve Boolean computing, such as the presented OR operator and the three-input device AND-OR logic operation. Importantly, these organometallic molecular wire-based logic gates can be simply reset by introduction of visible light, ensuring

the cycled set–reset operation. Although such logic computing cannot achieve logic flow through sequential gates so far, as the other chemical system-based approaches[57], the proof-of-concept of logic gate demonstrated here still provides a solid platform for the development of multifunctional molecular devices after optimizing fabrication and operative conditions.

Methods

Synthesis and molecular studies. Reactions were all achieved by using the Schlenk techniques, under an inert atmosphere. Solvents were freshly distillated under argon using standard procedures. The synthesis of the binuclear compound, *trans*-[AcS–*p*-C_6H_4–C≡C–$(dppe)_2$Ru–C≡C–(DTE)–C≡C–Ru$(dppe)_2$–C≡C–*p*-C_6H_4–SAc] (**1o**), was previously reported[44], and that of the new trinuclear compound, *trans*-[AcS–*p*-C_6H_4–C≡C–$(dppe)_2$Ru–C≡C–$(C_{15}S_2F_6H_8)$–C≡C–Ru$(dppe)_2$–C≡C–$(C_{15}S_2F_6H_8)$–C≡C–Ru$(dppe)_2$–C≡C–*p*-C_6H_4–SAc] (**2oo**), was based on the precursors H–C≡C–$(C_{15}S_2F_6H_6)$–C≡C–Ru$(dppe)_2$–C≡C–$(C_{15}S_2F_6H_6)$–C≡C–H (**3**)[41] and [$(dppe)_2$Ru = C = CHC_6H_4SAc](OTf) (**4**)[44] (Supplementary Fig. 5). In one Schlenk tube, complex **3** (32 mg, 0.02 mmol) was dried under vacuum for 30 min before addition of dichloromethane (20 ml) and triethylamine (4.0 ml, 0.37 mmol). The solution was cannula-transferred into a second Schlenk tube containing the metal vinylidene **4** (54 mg, 0.04 mmol) and $NaPF_6$ (12 mg, 0.07 mmol), also previously dried under vacuum for 30 minutes. The reaction mixture was stirred at room temperature for 5 days. Then, the reaction mixture was washed with water (3 × 15 ml). The remaining solvent was removed under reduced pressure. The residue was taken up in dichloromethane (10 ml), and pentane (30 ml) was slowly added leading to the formation of a light brown precipitate that was washed with further pentane (2 × 15 ml) to obtain **2oo** (60 mg, 81%). Data for **2oo**: ^{1}H NMR (500 MHz, C_6D_6, 297 K) δ: 7.73–6.92 (*m*, 128 H, $C_6H_5 + C_6H_4$-p-$SCOCH_3$), 6.83 (*s*, 2H, H_{DTE}), 6.74 (*s*, 2H, H_{DTE}), 2.47 (*m*, 24H, PCH_2CH_2P), 2.00 (*s*, 12H, $CH_{3\ DTE}$) 1.92 (*s*, 6H, $COCH_3$). ^{31}P NMR (121 MHz, C_6D_6, 297 K) δ: 53.5 (*s*, $dppe_{remote}$), 53.4 (*s*, $dppe_{central}$). IR (KBr): $\nu = 1{,}702\ cm^{-1}$ (C = O), $2052\ cm^{-1}$ (C≡C). HR-MS FAB$^+$ 3872.5555 (*m/z*): ($[M]^{+\cdot}$, calcd 3,872.5623). Analysis for $C_{214}H_{174}F_{12}O_2P_{12}Ru_3S_6$,: C 66.69, H 4.43 (cacld: C 66.37, H 4.53). (Supplementary Fig. 6) **2cc** was then obtained after excitation at $\lambda = 350$ nm in the NMR tube. Data for **2cc**: ^{1}H NMR (500 MHz, CD_3Cl_3, 297 K) δ: 7.36–6.91 (*m*, 124H $C_6H_5 + o$-C_6H_4-p-$SCOCH_3$), 6.81 (*d*, $^3J_{HH} = 6.0$ Hz, 4H, m-C_6H_4-p-$SCOCH_3$), 6.34 (*s*, 2H, H_{DTE}), 6.24 (*s*, 2H, H_{DTE}), 2.59 (*m*, 24H, PCH_2CH_2P), 2.42 (*s*, 6H, $COCH_3$), 1.82 (*s*, 6H, $CH_{3\ DTE}$), 1.81 (*s*, 6H, $CH_{3\ DTE}$). ^{31}P NMR (121 MHz, $CDCl_3$, 297 K) δ: 53.0 (*s*, $dppe_{remote}$), 52.4 (*s*, $dppe_{central}$). (Supplementary Fig. 7)

High-resolution mass spectra (HR-MS) were recorded on a ZabSpecTOF (LSIMS at 4 kV) spectrometer. UV–vis irradiations were performed in toluene with a LS series Light Source of ABET Technologies, Inc (150 W xenon lamp), equipped with single wavelength light filters '350FS 10–25' and '750FS 40–25'. UV–vis-NIR spectra were recorded with a Cary 5000 apparatus. Electrochemical studies were carried out under argon using an Autolab PGSTAT 30 potentiostat (CH_2Cl_2, 0.2 M Bu_4NPF_6). The working electrode was a Pt disk and ferrocene the internal reference. It should be noted that all the reactions and handling of the compounds were carried out in the dark.

Device fabrication. Gold nanowires (~5 μm) with specific nanogaps (~3 nm, and ~5 nm corresponding to the actual length of **1** and **2**) were prepared following the standard procedures of OWL[45–47]. Au-Ni-Au multi-segment nanowires were firstly obtained by electrochemical deposition of commercial electroplating solutions (Ag: 1025 Silver, Ni: Nickel Sulphamate RTU and Au: Orotemp 24RTU, Technic Inc.) within an anodic aluminium oxide (AAO) porous membrane (Whatman, Anodisc 0.02 μm pores, 47 mm outer diameter) that was previously coated with 200 nm Ag layer on the reverse, as both the template and the working electrode. Ag was deposited as an initial electrical contact layer under DC current at −800 mV (versus Ag/AgCl), while nickel was plated at −850 mV and gold was plated at −950 mV to form nanowires. The thickness of the sacrificed layer (Ni) was charge-controlled by 10 mC for 1 nm. After Ag contact layer and AAO template were sequentially dissolved, plasma-enhanced chemical vapour deposition was used to deposit ~50 nm silica on the wire surface. Finally, the sacrificial layer of Ni was etched by 1 M HCl for 3 h, and then a ~3 nm or a ~5 nm gap was generated in the 5-μm nanorod for the assembly of functional molecules.

The outer gold microeletrodes were patterned via standard processes of photolithography on a Si/SiO_2 chip. Then, after being deposited onto a chip with patterned gold microeletrodes, the two ends of the fabricated nanowire were connected to microelectrodes using e-beam lithography and sequential metal deposition of 5 nm Cr and 400 nm Au. (See Supplementary Methods for details). SEM (JEOL JSM-7600F) was employed to observe the morphology of the nanodevices and to measure the size of the nanogap.

Functional molecule assembly. The fabricated nanogap devices were cleaned using oxygen plasma for 5 min. The wafer was then immersed in the 5 ml degassed THF solution containing 1 mg **1c** or **2cc** in the dark for 24 h, and under N_2 atmosphere. This THF solution of **1c** or **2cc** was obtained by the following method: (1) The THF solution of precursor open state molecules, **1o** or **2oo**, was irradiated with 365 nm UV light for 30 min to ensure that all the open molecules switched to closed state; (2) the degassed solution of **1c** or **2cc** NH_4OH (28% of NH_3, 5 μl) was added dropwise for deprotection of the thiol. The wafer with nanogap devices was further rinsed with THF and ethanol, and then dried with N_2. It should be noted that the more rigid closed state molecules were preferred to the unfavourable molecular conformation of the open state molecules (less linear and rigid) to form active MTJs (Supplementary Fig. 8)[44]. As the gold nanorod is of 300 nm in diameter, the accessible surface is thus roughly of $7 \times 10^4\ nm^2$ if the surface is considered as planar (minimum surface). The molecules have a diameter of 1.5 nm (ref. 44), if grafted perpendicularly to the electrode surface, thus roughly of $2.25\ nm^2$ in surface. Therefore, a maximum number of $\sim 3 \times 10^4$ molecules could be ideally assembled in the junction.

External stimulations. UV–vis irradiation was performed with a 150 W xenon lamp with single wavelength light filters at 365 nm (30 min) and 700 nm (2 h). All electrochemical stimuli were performed using an electrochemical analyser, model 832C (CH Instruments). Electrolysis for DTE cyclization were carried at 0.45 V (10 min) for oxidation and −0.05 V (10 min) for reduction in CH_2Cl_2 with a three-electrode system consisting of the gold nanoelectrode as working electrode, a platinum wire counter electrode and a Ag/AgCl reference electrode.

Electrical measurements. The current–voltage characteristics of the multi-modulated nanodevices were obtained in solid state using a semiconductor parameter analyser (Keithley 4200-SCS) for the application of a potential and measurement of currents, combined with a cryogen-free micromanipulated probe station (Janis CCR-12) for connecting the microelectrodes. Unless otherwise stated, the measurements were conducted under vacuum (1×10^{-4} torr).

References

1. Aviram, A. & Ratner, M. A. Molecular rectifiers. *Chem. Phys. Lett.* **29,** 277–283 (1974).
2. Heath, J. R. & Ratner, M. A. Molecular electronics. *Phys. Today* **56,** 43–49 (2003).
3. Nitzan, A. & Ratner, M. A. Electron transport in molecular wire junctions. *Science* **300,** 1384–1389 (2003).
4. Tao, N. J. Electron transport in molecular junctions. *Nat. Nanotech.* **1,** 173–181 (2006).
5. Choi, S. H., Kim, B. & Frisbie, C. D. Electrical resistance of long conjugated molecular wires. *Science* **320,** 1482–1486 (2008).
6. Liu, Z. *et al.* Revealing the molecular structure of single molecule junctions in different conductance states by fishing-mode tip-enhanced Raman spectroscopy. *Nat. Commun.* **2,** 305 (2011).
7. Metzger, R. M. *et al.* Unimolecular electrical rectification in hexadecylquinolinium tricyanoquinodimethanide. *J. Am. Chem. Soc.* **119,** 10455–10466 (1997).
8. Nijhuis, C. A., Reus, W. F., Barber, J. R., Dickey, M. D. & Whitesides, G. M. Charge transport and rectification in arrays of SAM-based tunneling junctions. *Nano Lett.* **10,** 3611–3619 (2010).
9. Chen, J., Reed, M. A., Rawlett, A. M. & Tour, J. M. Large on-off ratios and negative differential resistance in a molecular electronic device. *Science* **286,** 1550–1552 (1999).
10. Zhou, L. P. *et al.* One-dimensional iron − cyclopentadienyl sandwich molecular wire with half metallic, negative differential resistance and high-spin filter efficiency properties. *J. Am. Chem. Soc.* **130,** 4023–4027 (2008).
11. Park, J. *et al.* Coulomb blockade and the Kondo effect in single-atom transistors. *Nature* **417,** 722–725 (2002).
12. Kronemeijer, A. J. *et al.* Reversible conductance switching in molecular devices. *Adv. Mater.* **20,** 1467–1473 (2008).
13. Uchida, K., Yamanoi, Y., Yonezawa, T. & Nishihara, H. Reversible on/off conductance switching of single diarylethene immobilized on a silicon surface. *J. Am. Chem. Soc.* **133,** 9239–9241 (2011).
14. Tam, E. S. *et al.* Single-molecule conductance of pyridine-terminated dithienylethene switch molecules. *ACS Nano* **5,** 5115–5123 (2011).
15. Aradhya, S. V. *et al.* Dissecting contact mechanics from quantum interference in single-molecule junctions of stilbene derivatives. *Nano Lett.* **12,** 1643–1647 (2012).
16. Ikeda, M., Tanifuji, N., Yamaguchi, H., Irie, M. & Matsuda, K. Photoswitching of conductance of diarylethene-Au nanoparticle network. *Chem. Commun.* 1355–1357 (2007).
17. Li, C. *et al.* Charge transport in single Au | alkanedithiol | Au junctions: coordination geometries and conformational degrees of freedom. *J. Am. Chem. Soc.* **130,** 318–326 (2008).
18. Kim, Y. *et al.* Conductance and vibrational states of single-molecule junctions controlled by mechanical stretching and material variation. *Phys. Rev. Lett.* **106,** 196804 (2011).

19. Pasupathy, A. N. *et al.* The Kondo effect in the presence of ferromagnetism. *Science* **306,** 86–89 (2004).
20. Cho, W. J., Cho, Y., Min, S. K., Kim, W. Y. & Kim, K. S. Chromium porphyrin arrays as spintronic devices. *J. Am. Chem. Soc.* **133,** 9364–9369 (2011).
21. Collier, C. P. *et al.* A [2]catenane-based solid state electronically reconfigurable switch. *Science* **289,** 1172–1175 (2000).
22. Kubatkin, S. *et al.* Single-electron transistor of a single organic molecule with access to several redox states. *Nature* **425,** 698–701 (2003).
23. Miyamachi, T. *et al.* Robust spin crossover and memristance across a single molecule. *Nat. Commun.* **3,** 938 (2012).
24. Xu, B. Q., Li, X. L., Xiao, X. Y., Sakaguchi, H. & Tao, N. J. Electromechanical and conductance switching properties of single oligothiophene molecules. *Nano Lett.* **5,** 1491–1495 (2005).
25. Díez-Pérez, I. *et al.* Ambipolar transport in an electrochemically gated single-molecule field-effect transistor. *ACS Nano* **6,** 7044–7052 (2012).
26. He, J., Fu, Q., Lindsay, S., Ciszek, J. W. & Tour, J. M. Electrochemical origin of voltage-controlled molecular conductance switching. *J. Am. Chem. Soc.* **128,** 14828–14835 (2006).
27. Li, Z., Liu, Y., Mertens, S. F., Pobelov, I. V. & Wandlowski, T. From redox gating to quantized charging. *J. Am. Chem. Soc.* **16,** 8187–8193 (2010).
28. Janin, M., Ghilane, J. & Lacroix, J.-C. When electron transfer meets electron transport in redox-active molecular nanojunctions. *J. Am. Chem. Soc.* **135,** 2108–2111 (2013).
29. Uehara, M., Mori, S., Chen, C. H. & Cheong, S.-W. Percolative phase separation underlies colossal magnetoresistance in mixed-valent manganites. *Nature* **399,** 560–563 (1999).
30. Yang, M., Oró-Solé, J., Kusmartseva, A., Fuertes, A. & Attfield, J. P. Electronic tuning of two metals and colossal magnetoresistances in $EuWO_{1+x}N_{2-x}$ perovskites. *J. Am. Chem. Soc.* **132,** 4822–4829 (2010).
31. Noh, Y. Y. *et al.* Effect of light irradiation on the characteristics of organic field-effect transistors. *J. Appl. Phys.* **100,** 094501 (2006).
32. Ye, C. *et al.* Multilevel conductance switching of memory device through photoelectric effect. *J. Am. Chem. Soc.* **134,** 20053–20059 (2012).
33. Irie, M. Diarylethenes for memories and switches. *Chem. Rev.* **100,** 1685–1716 (2000).
34. Kim, Y. *et al.* Charge transport characteristics of diarylethene photoswitching single-molecule junctions. *Nano Lett.* **12,** 3736–3742 (2012).
35. Mahapatro, A. K., Ying, J., Ren, T. & Janes, D. B. Electronic transport through ruthenium-based redox-active molecules in metal-molecule-metal nanogap junctions. *Nano Lett.* **8,** 2131–2136 (2008).
36. Olivier, C. *et al.* 'Chain-like' trimetallic ruthenium complexes with C_7 carbon-rich bridges: experimental and theoretical investigations of electronic communication tuning in five distinct oxidation states. *J. Am. Chem. Soc.* **132,** 5638–5651 (2010).
37. Norel, L. *et al.* A carbon-rich ruthenium decorated dysprosium single molecule magnet. *Chem. Commun.* **48,** 3948–3950 (2012).
38. Di Piazza, E. *et al.* d – f Heterobimetallic association between ytterbium and ruthenium carbon-rich complexes: redox commutation of near-IR luminescence. *J. Am. Chem. Soc.* **133,** 6174–6176 (2011).
39. Rigaut, S. Metal complexes in molecular junctions. *Dalton Trans.* **42,** 15859–15863 (2013).
40. Liu, Y. *et al.* A multifunctional organometallic switch with carbon-rich ruthenium and diarylethene units. *Chem. Commun.* 6117–6119 (2008).
41. Hervault, Y.-M., Ndiaye, C. M., Norel, L., Lagrost, C. & Rigaut, S. Controlling the stepwise closing of identical DTE photochromic units with electrochemical and optical stimuli. *Org. Lett.* **14,** 4454–4457 (2012).
42. Li, B., Wang, J.-Y., Wen, H.-M., Shi, L.-X. & Chen, Z.-N. Redox-modulated stepwise photochromism in a ruthenium complex with dual dithienylethene-acetylides. *J. Am. Chem. Soc.* **134,** 16059–16067 (2012).
43. Green, K. A., Cifuentes, M. P., Corkery, T. C., Samoc, M. & Humphrey, M. G. Switching the cubic nonlinear optical properties of an electro-, halo-, and photochromic ruthenium alkynyl complex across six states. *Angew. Chem. Int. Ed.* **48,** 7867–7870 (2009).
44. Meng, F. *et al.* Photo-modulable molecular transport junctions based on organometallic molecular wires. *Chem. Sci.* **3,** 3113–3118 (2012).
45. Qin, L., Park, S., Huang, L. & Mirkin, C. A. On-wire lithography. *Science* **309,** 113–115 (2005).
46. Qin, L., Jang, J. W., Huang, L. & Mirkin, C. A. Sub-5-nm gaps prepared by On-wire lithography: correlating gap size with electrical transport. *Small* **3,** 86–90 (2007).
47. Osberg, K. D., Schmucker, A. L., Senesi, A. J. & Mirkin, C. A. One-dimensional nanorod arrays: independent control of composition, length, and interparticle spacing with nanometer precision. *Nano Lett.* **11,** 820–824 (2011).
48. Dulic, D. *et al.* One-way optoelectronic switching of photochromic molecules on gold. *Phys. Rev. Lett.* **91,** 207402 (2003).
49. Moriyama, Y., Matsuda, K., Tanifuji, N., Irie, S. & Irie, M. Electrochemical cyclization/cycloreversion reactions of diarylethenes. *Org. Lett.* **7,** 3315–3318 (2005).
50. Gorodetsky, B. & Branda, N. R. Bidirectional ring-opening and ring-closing of cationic 1,2-dithienylcyclopentene molecular switches triggered with light or electricity. *Adv. Funct. Mater.* **17,** 786–796 (2007).
51. Chen, X. *et al.* On-wire lithography-generated molecule-based transport junctions: A new testbed for molecular electronics. *J. Am. Chem. Soc.* **130,** 8166–8168 (2008).
52. Chen, X. *et al.* Spectroscopic tracking of molecular transport junctions generated by using click chemistry. *Angew. Chem. Int. Ed.* **48,** 5178–5181 (2009).
53. Chen, X. *et al.* Chemical fabrication of heterometallic nanogaps for molecular transport junctions. *Nano Lett.* **9,** 3974–3979 (2009).
54. Meng, F. *et al.* Protein-based memristive nanodevices. *Small* **7,** 3016–3020 (2011).
55. Ramachandran, G. K. *et al.* A bond-fluctuation mechanism for stochastic switching in wired molecules. *Science* **300,** 1413–1416 (2003).
56. Vericat, C., Vela, M. E., Benitez, G., Carro, P. & Salvarezza, R. C. Self-assembled monolayers of thiols and dithiols on gold: new challenges for a well-known system. *Chem. Soc. Rev.* **39,** 1805–1834 (2010).
57. de Silva, A. P. & Uchiyama, S. Molecular logic and computing. *Nat. Nanotech.* **2,** 399–410 (2007).
58. Tybrandt, K., Forchheimer, R. & Berggren, M. Logic gates based on ion transistors. *Nat. Commun.* **3,** 871 (2012).
59. Katz, E. & Privman, V. Enzyme-based logic systems for information processing. *Chem. Soc. Rev.* **39,** 1835–1857 (2010).
60. Wang, B., Kitney, R. I., Joly, N. & Buck, M. Engineering modular and orthogonal genetic logic gates for robust digital-like synthetic biology. *Nat. Commun.* **2,** 508 (2011).
61. Elbaz, J., Wang, Z. G., Orbach, R. & Willner, I. pH-stimulated concurrent mechanical activation of two DNA 'tweezers'. A 'SET – RESET' logic gate system. *Nano Lett.* **9,** 4510–4514 (2009).
62. Pischel, U., Uzunova, V. D., Remón, P. & Nau, W. M. Supramolecular logic with macrocyclic input and competitive reset. *Chem. Commun.* **46,** 2635–2637 (2010).
63. Tian, F., Jiao, D., Biedermann, F. & Scherman, O. A. Orthogonal switching of a single supramolecular complex. *Nat. Commun.* **3,** 1207 (2012).
64. Kumar, A. S. *et al.* Reversible photo-switching of single azobenzene molecules in controlled nanoscale environments. *Nano Lett.* **8,** 1644–1648 (2008).

Acknowledgements

We first sincerely appreciate Dr Karine Costuas's help (Rennes) for the calculation of molecular length of **2cc**. We also thank the support from the National Research Foundation of Singapore (NRF-RF2009-04 and the Singapore-Berkeley Initiative for Sustainable Energy), Singapore Ministry of Education Tier2 (MOE2010-T2-1-017), the Merlion programme, the Université de Rennes 1, the CNRS and the ANR (ANR-09-JCJC-0025).

Author contributions

X.C. and S.R. proposed the concept. F.M., S.R. and X.C. designed the experiment. Y.-M.H., L.N. and S.R. synthesized the molecules. F.M., Q.S. and B.H. fabricated the nanodevices. F.M., S.R., Y.-M.H., L.N. and X.C. discussed the results, and co-wrote the manuscript.

Additional information

Supplementary Information accompanies this paper at http://www.nature.com/naturecommunications

Competing financial interests: The authors declare no competing financial interests.

Reprints and permission information is available online at http://npg.nature.com/reprintsandpermissions/

How to cite this article: Meng, F. *et al.* Orthogonally modulated molecular transport junctions for resettable electronic logic gates. *Nat. Commun.* 5:3023 doi: 10.1038/ncomms4023 (2014).